Influence of Vapour Bubbles Size and Spacing on Droplet Impact Outcomes under Subcooled Boiling Regimes

Daniel Vasconcelos*[1], André Silva[1], Jorge Barata[1]
[1]Universidade da Beira Interior, Covilhã, 6200-001, Portugal
*Corresponding author: daniel.vasconcelos.rodrigues@ubi.pt

Abstract
Multiphase flows are characterised as heterogeneous mixtures of two or more phases, such as gas-liquid or solid-liquid. These are extremely complex due to the underlying dynamics that may occur, which include interfacial phenomena, such as boiling and evaporation, and interactions between phases. Specifically, droplet impact onto heated wetted surfaces has been overlooked in the literature, which involves heat and mass transfer mechanisms related to sensible heating, condensation and evaporation. The droplet impact phenomenon occurs in several industrial applications, such as internal combustion engines, electronics cooling devices, heat exchangers, among others. In numerical terms, improving efficiency and reliability of simulations is of interest to understand the behaviour of mathematical models for complex physical systems. The main objective of this work is to numerically simulate droplet impact onto a heated liquid film in the presence of vapour bubbles in a 2D-axisymmetric assumption. The numerical model solves the incompressible mass, momentum and energy equations coupled with the VOF method and height functions for accurately capturing the interface. Phase-change processes such as evaporation and condensation are neglected for the current simulations. Water and n-decane are the fluids adopted for the simulation. The impact conditions are $D_0 = 3.0\ mm$, $h^* = 0.5$, and $U_0 = 3.0\ m/s$. Different vapour bubble sizes, (D_v), and spacings, (x_v), are studied to evaluate the vapour bubble phenomena and crown geometrical parameters. An initial vapour bubble is positioned on the axis of symmetry, $x_s = 0$, and, therefore, in the droplet trajectory. Results indicate that vapour bubbles have a lower influence on crown diameter, and a higher influence on crown height. Increasing the size of vapour bubbles leads to a decrease in both crown diameter and height, whereas an increase in the vapour bubbles spacing causes an increase in the crown height and diameter. The initial vapour bubble positioning in relation to the axis of symmetry is a factor that should also be considered in future studies.

Keywords
Numerical Simulation, Droplet Impact, Vapour Bubbles, Subcooled Boiling Regime

Introduction

Nowadays, interfacial phenomena have become increasingly important due to the heat and mass transfer potential associated with evaporation/condensation. These are included in multiphase flows, which are characterised as heterogeneous mixtures of two or more phases, such as gas-liquid or solid-liquid. On this topic, the droplet impact phenomenon occurs in several industrial applications, such as internal combustion engines with direct fuel injection, electronics cooling devices and heat exchangers. However, numerically simulating these flows is still extremely complex and requires further studies regarding flow dynamics, and mass and heat transfer.

Several authors have conducted research on this field. Guo et al. [1] performed 2D numerical simulations to study the evolution of vapour bubbles and their influence on convective heat transfer. Several bubble dynamics were visualised, such as bubble merging and entrapment, and liquid film break-up. The evolution of vapour bubbles for different liquid film thicknesses is remarkably different, ranging from bubble detachment and surface break-up for lower thicknesses, to bubble flow and merge for higher thicknesses. Liang et al. [2] studied both successive and simultaneous droplets impact onto a liquid film heated by conduction. The CLSVOF

method is employed to capture the liquid-gas interface, and no phase-change processes are considered. Results show that the heat transfer coefficient on the impact region is higher than on the undisturbed liquid film, and several blind spots were spotted under the central sheet due to flow stagnation and higher local thickness. More recently, Liang et al. [3] also focused on single and multi-droplet impact, considering the phase-change model proposed by Lee [4] and different vapour bubbles initial configuration. These bubbles may cause film rupture if the expanding crown contacts the pre-existing bubbles, leading to the crown disintegration. The authors state that a decrease in the contact angle can promote bubble detachment and improve boiling heat transfer performance, and the heat transfer coefficient on the impact crater is lower than on the interaction region and developing crown due to the increased number of vapour bubbles present in those spots. In terms of asymmetric droplet impact, Wang et al. [5] analysed heat transfer characteristics and impact dynamics of a double droplet onto a moving liquid film. The authors state that a higher local wall heat flux is obtained for higher impact velocities, smaller droplet spacing, and thinner liquid films.
The main objective of this work is to numerically simulate droplet impact onto a heated liquid film in the presence of vapour bubbles in a 2D-axisymmetric assumption. Several vapour bubble sizes, D_v, and spacings, x_v, are studied to evaluate crown morphology.

Numerical Model
The numerical model solves the 2D-axisymmetric incompressible Navier-Stokes equations coupled with the VOF method for two-phase flows. In order to perform these computations, the open-source CFD software Basilisk was adopted. This software deals with solving partial differential equations under adaptive Cartesian grids. The continuity, momentum and energy equations that define our model are represented by equations (1), (2) and (3), respectively:

$$\nabla \cdot \vec{U} = 0 \tag{1}$$

$$\frac{\partial}{\partial t}\left(\rho\vec{U}\right) + \nabla \cdot \left(\rho\vec{U}\vec{U}\right) = -\nabla p + \nabla \cdot \left[\mu\left(\nabla\vec{U} + \nabla\vec{U}^{\mathsf{T}}\right)\right] + \rho\vec{g} - \vec{F_\sigma} \tag{2}$$

$$\frac{\partial}{\partial t}\left(\rho T\right) + \nabla \cdot \left(\rho\vec{U}T\right) = \nabla \cdot \left(\frac{k}{C_p}\nabla T\right) \tag{3}$$

where U is velocity, ρ is density, p is pressure, μ is viscosity, $\vec{g}$ is the gravitational acceleration constant, F_σ are surface tension forces, T is temperature, k is thermal conductivity and C_p is heat capacity. The VOF method is employed to track the liquid-gas interface between the phases. These distinct phases are defined by the volume fraction scalar, α, which varies between $\alpha = 0$ for the gas phase, and $\alpha = 1$ for the liquid phase. The interface of the two-phase flow is represented by values of $0 < \alpha < 1$. The scalar advection equation for the volume fraction is given by eq. (4):

$$\frac{\partial \alpha}{\partial t} + \nabla \cdot \left(\vec{U}\alpha\right) = 0 \tag{4}$$

Surface tension is modelled as an explicit term in the momentum equation by the continuum surface force (CSF) model [6], and is displayed by eq. (5):

$$F_\sigma = \sigma\kappa\delta_s\vec{n} \tag{5}$$

where σ is the surface tension, κ is the interface curvature, δ_s is a Dirac distribution function, and $\vec{n}$ is the normal of the interface. The curvature and normal calculation are based on height-functions [7] rather than the volume fraction. The respective equations are presented by eq. (6) and eq. (7):

$$\kappa = \frac{h_{xx}}{\left(1 + h_x^2\right)^{3/2}} \tag{6}$$

$$\vec{n} = (h_x, -1) \tag{7}$$

The physical properties of the liquid and gas phases must be defined on the numerical field and are calculated as a function of the volume fraction scalar. An arithmetic mean is defined for the density calculation, represented by eq. (8), whereas the viscosity, thermal conductivity and heat capacity are estimated through harmonic means. These are displayed by eq. (9), (10) and (11), respectively:

$$\rho = \alpha\rho_l + (1 - \alpha)\,\rho_g \tag{8}$$

$$\mu = \frac{1}{\frac{\alpha}{\mu_l} + \frac{1-\alpha}{\mu_g}} \tag{9}$$

$$k = \frac{1}{\frac{\alpha}{k_l} + \frac{1-\alpha}{k_g}} \tag{10}$$

$$C_p = \frac{1}{\frac{\alpha}{C_{p_l}} + \frac{1-\alpha}{C_{p_g}}} \tag{11}$$

where the subscript g corresponds to the gas phase, and l to the liquid phase. Figure 1 exhibits a schematic of the physical setup. A single droplet, of diameter D_0 and impact velocity U_0, impinges onto a liquid film of thickness h. Within the liquid film, there is the presence of vapour bubbles. These can be defined by the vapour bubble spacing, x_v, vapour bubble diameter, D_v, and initial vapour bubble displacement, x_s. These bubbles are set as gas phase $(\alpha = 0)$ for numerical simplification. Gravity forces are enabled and act on the negative direction of the y-axis. Water and n-decane are the fluids adopted for the liquid phase, and its thermophysical properties are defined on table 1 for the temperatures established on the numerical simulations. The droplet is set at ambient temperature, whereas the liquid film is heated. For water, the liquid film temperature, T_f, is equal to $T_f = 50\ ^\circ$C and, for n-decane, $T_f = 80\ ^\circ$C. These temperatures were chosen based on a dimensionless temperature of $\theta \approx 0.4$. This parameter correlates the temperatures of the liquid film, T_f, the surrounding air, T_{air}, and the saturation temperature of the fluid, T_{sat}, as represented by eq. (12).

$$\theta = \left(T_f - T_{air}\right) / \left(T_{sat} - T_{air}\right) \tag{12}$$

These numerical simulations are performed on the simplifying assumption that the thermophysical properties are constant. For the liquid phase, the droplet and the liquid film assume the physical properties of the heated liquid film. The physical properties of air are $\rho_g = 1.225\ kg/m^3$ and $\mu_g = 1.789 \times 10^{-2}\ mPa.s$ at ambient temperature. The computational domain is a quadrilateral with four different boundary conditions. The left boundary is defined as the axis of

symmetry and it is used as the centreline for the axisymmetric simulations. The top and right boundaries are pressure-outlets to represent the far-field. The bottom boundary is the impact surface, characterised by a no-slip condition for the velocity, and a fixed wall temperature equal to the liquid film temperature. The simulations are resolved on a Cartesian adaptive mesh, refining the liquid-gas interface and coarsening the outer regions. In order to solve the Navier-Stokes equations, an approximate projection method for the pressure-velocity coupling and a momentum-conserving advection scheme for the velocity are employed. For the interface reconstruction, a PLIC-based scheme for the liquid-gas interface is adopted. The independence studies for mesh, time and domain were performed in a previous study [8]. Therefore, a quadrilateral with height and radial distance of $5.3D_0$, a CFL condition of CFL $= 0.5$, and a mesh resolution of 92 cells per diameter were defined for the numerical simulations.

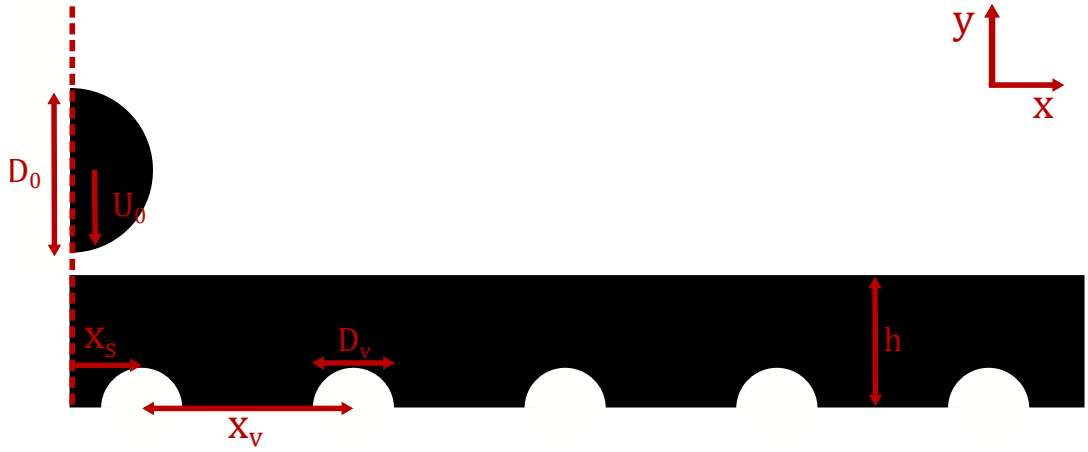

Figure 1. Numerical setup: x_s - Initial vapour bubble displacement from axis of symmetry; D_0 - Droplet diameter; U_0 - Droplet impact velocity; D_v - Vapour bubble diameter; x_v - Vapour bubble spacing; h - Liquid film thickness.

Fluid	T_f $[^\circ C]$	ρ $[kg/m^3]$	μ $[mPa.s]$	σ $[mN/m]$	k $[J/\,(m.s.K)]$	C_p $[J/\,(Kg.K)]$
Water	50	988.0	0.547	67.94	0.631	4181.0
N-decane	80	686.1	0.449	18.25	0.119	2332.5

Table 1. Thermophysical properties for water and n-decane at atmospheric pressure.

Results and Discussion

The following results will be presented both qualitative and quantitatively. In qualitative terms, crown evolution and temperature fields will be presented. For the quantitative work, crown diameter and height measurements are analysed for different vapour bubbles size and spacing. The impact conditions for water and n-decane are $D_0 = 3.0\ mm$, $U_0 = 3.0\ m/s$, and $h^* = h/D_0 = 0.5$. There are three parameters regarding vapour bubbles, which consist of the vapour bubble initial displacement, x_s, diameter, D_v, and spacing, x_v. For these numerical simulations, no initial displacement was considered and, therefore, $x_s = 0$. For the remaining parameters, four different vapour bubble sizes and three spacings were simulated, which include $D_v^* = D_v/D_0 = 1/2$, $D_v^* = 1/3$, $D_v^* = 1/5$, $D_v^* = 1/10$, and $x_v^* = x_v/D_0 = 1/2$, $x_v^* = 1$, $x_v^* = 2$.
Figure 2 shows the visualisation of a water droplet onto a heated liquid film for $D_v^* = 1/3$ and $x_v^* = 0.5$ for different stages of the impact. The dimensionless time is defined by $\tau = tU_0/D_0$ and is used to characterise the phenomenon. The moment of impact is defined by $\tau = 0$. For $\tau = 2.5$, there is a crown formation with secondary atomisation. In terms of vapour bubbles, it is possible to visualise the bubble detachment from two bubbles near the crown base, which may lead to both bubbles merging, as it occurs on the following frame for $\tau = 3$. For $\tau = 5$, this

vapour bubble contacts into the crown, shattering its base, which may lead to lower values of height and diameter at later stages due to the crown disintegration.

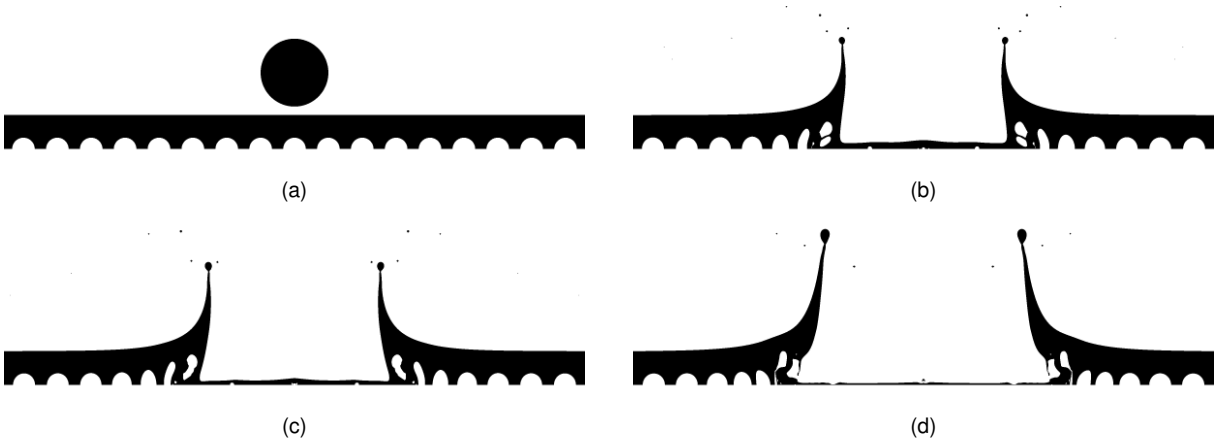

Figure 2. Water droplet impact onto a heated liquid film for different time frames for $D_v^* = 1/3$ and $x_v^* = 0.5$: (a) $\tau = 0$; (b) $\tau = 2.5$; (c) $\tau = 3$; (d) $\tau = 5$.

Figures 3a and 3b present the dimensionless crown height, $H^* = H/D_0$, and outer diameter, $D_{out}^* = D_{out}/D_0$, measurements as a function of dimensionless time for $x_v^* = 1.0$. According to the results presented, a decrease in the vapour bubbles size leads to an increase in both crown height and diameter. For higher vapour bubble sizes, such as $D_v^* = 1/2$ and $D_v^* = 1/3$, the crown tends to decrease its height at earlier stages when compared to lower bubble sizes. It is also possible to visualise a sudden decrease of the crown diameter for $D_v^* = 1/2$, which is due to a bubble contacting with the crown at earlier stages of the impact.

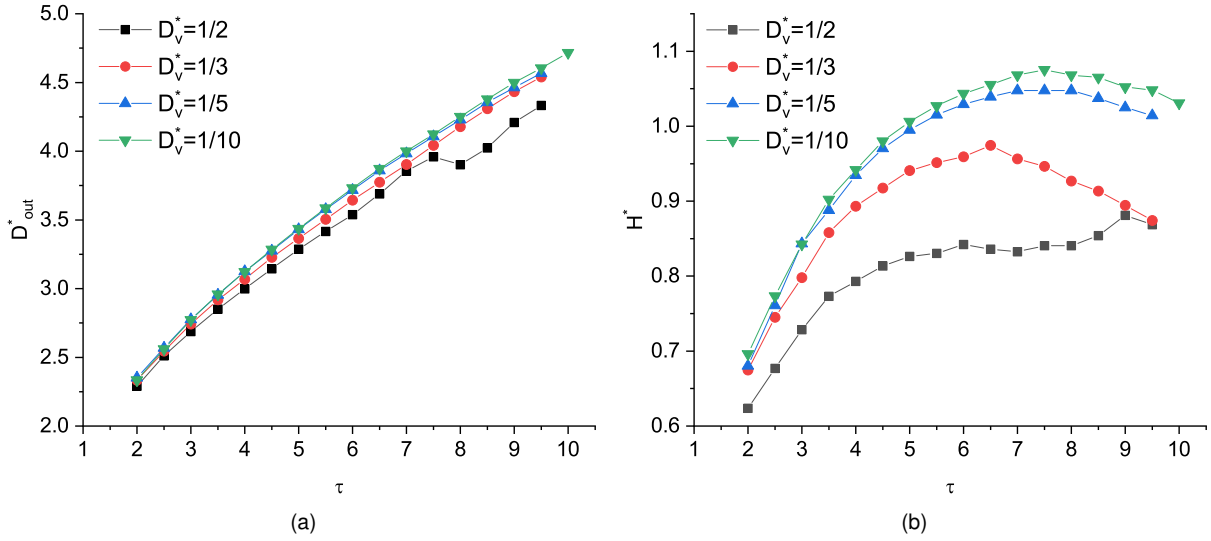

Figure 3. Crown measurements for water droplet impact for $x_v^* = 1.0$: a) Dimensionless crown outer diameter; b) Dimensionless crown height.

Figures 4a and 4b display the dimensionless crown height, $H^* = H/D_0$, and crown outer diameter, $D_{out}^* = D_{out}/D_0$, measurements as a function of dimensionless time for the droplet impact of n-decane for $D_v^* = 1/5$. The results show a tendency where the increase of the vapour bubble spacing causes the crown geometrical properties to also increase. Despite that, for figure 4a, the crown outer diameter for the condition of $x_v^* = 1.0$ are slightly lower than for $x_v^* = 2.0$, which can be related to the crown rim instabilities associated with the n-decane low surface tension at this temperature. For both water and n-decane, the influence of the vapour bubbles is lower on the crown outer diameter and higher for the crown height, despite showing similar tendencies.

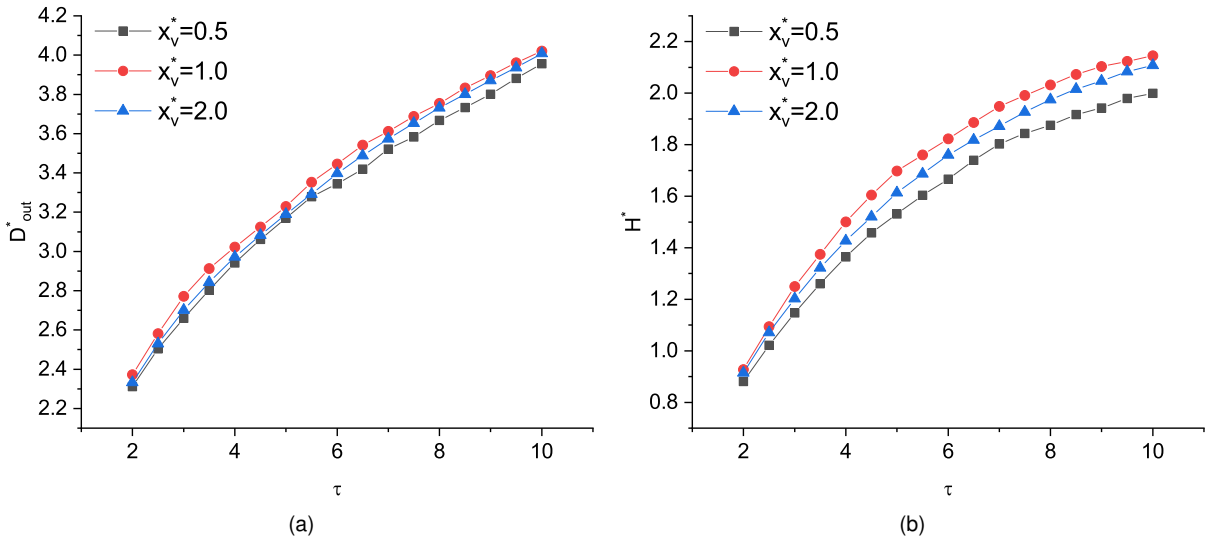

Figure 4. Crown measurements for n-decane droplet impact for $D_v^* = 1/5$: a) Dimensionless crown outer diameter; b) Dimensionless crown height.

In terms of fluid comparison, figures 5a and 5b display the crown height measurements for both water and n-decane considering $D_v^* = 1/3$. Due to the fluids difference in thermophysical properties, most significantly the surface tension, the crown height for water is significantly lower when compared to n-decane. For water, the crown reaches its maximum height between $\tau = 5$ for the smaller vapour bubble sizes, and $\tau = 8$ for higher sizes, whereas for n-decane, the crown is still developing until reaching its maximum height and, afterwards, slowly decrease until the crown potentially shatters. Nevertheless, both fluids show a similar tendency, in which an increase in the vapour bubble sizes causes an increase in the crown height.

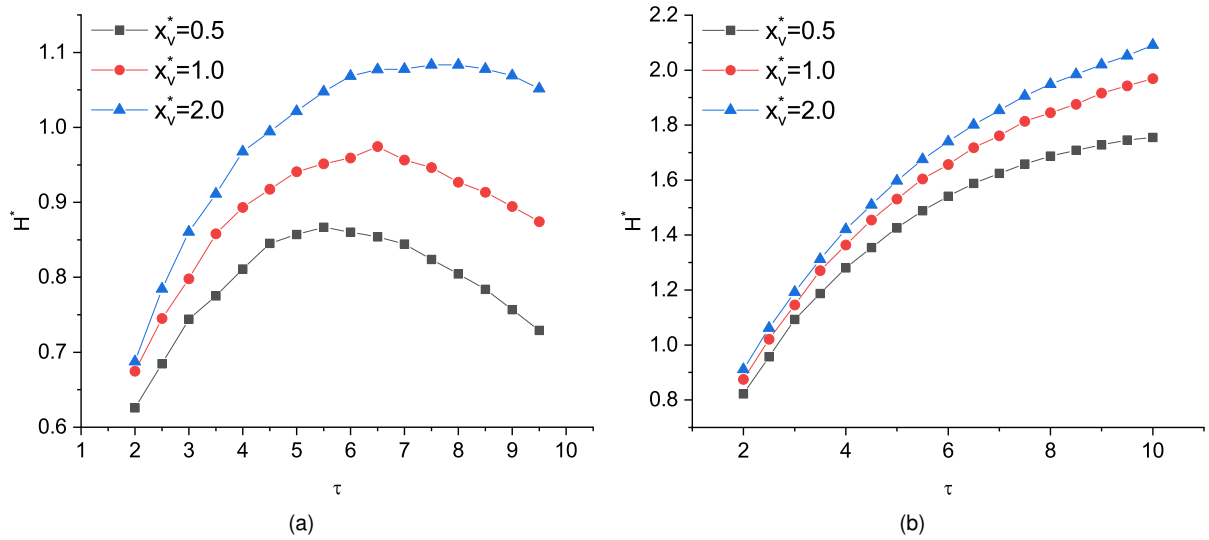

Figure 5. Dimensionless crown height measurements for droplet impact for $D_v^* = 1/5$: a) Water; b) N-decane.

A parameter that should be considered for future studies is the initial vapour bubble displacement, x_s, in order to understand if the initial bubbles detachment and posterior collapse with the crown is promoted or suppressed by the position in which these phenomena occur. Moreover, the influence of film temperature should be evaluated in terms of thermophysical properties and local evaporation/condensation, coupled with the presented results.

Conclusions

The influence of vapour bubbles size and spacing was analysed both qualitative and quantitatively. In qualitative terms, several outcomes were visualised, such as vapour bubble detachment from the impact surface, bubble merging, and bubble collapse with the crown, which may lead to its posterior disintegration. Quantitatively, results show indicate that vapour bubbles have a lower influence on crown outer diameter, and a higher influence on crown height. Increasing the size of vapour bubbles leads to a decrease in both crown diameter and height for most of the cases, whereas an increase in the bubbles spacing causes an increase in the crown height and diameter. The initial vapour bubble positioning in relation to the axis of symmetry and the influence of temperature are factor that should be considered in future studies.

Acknowledgements

The present work was performed under the scope of Aeronautics and Astronautics Research Center (AEROG) of the Laboratório Associado em Energia, Transportes e Aeronáutica (LAETA) activities, supported by Fundação para a Ciência e Tecnologia (FCT) through the project number UIDB/50022/2020 and by the Ph.D. scholarship with the reference SFRH BD/143307/2019.

References

[1] Guo, Y., Wang, F., Gong, L., Shen, S., 2019, *Numerical Heat Transfer, Part B: Fundamentals*, 76(5), 273-284.

[2] Liang, G., Zhang, T., Chen, L., Chen, Y., Shen, S., 2019, *International Journal of Heat and Mass Transfer*, 132, 288-292.

[3] Liang, G., Zhang, T., Chen, Y., Chen, L., Shen, S., 2019, *International Journal of Heat and Mass Transfer*, 139, 832-847.

[4] Lee, W. H., 1980, *Multiphase Transport: Fundamentals, Reactor Satefy, Applcations*, 407-432.

[5] Wang, Y. B., Wang, X. D., Wang, T. H., Yan, W. M., 2018, *International Journal of Heat and Mass Transfer*, 126, 649-659.

[6] Brackbill, J. U., Kothe, D. B., Zemach, C., 1992, *Journal of computational physics*, 100(2), 335-354.

[7] Popinet, S., 2009, *Journal of Computational Physics*, 228(16), 5838-5866.

[8] Vasconcelos, D., Silva, A., Barata, J., 29 Aug. - 2 Sept., 2021, *15th Triennial International Conference on Liquid Atomization and Spray Systems.*